The Role of Aluminum on the Weldability and Sulfidation Behavior of Iron-Aluminum Cladding

The study showed cracking of Fe-Al cladding was independent of the welding process and parameters, but related directly to the amount of aluminum present

BY S. W. BANOVIC, J. N. DuPONT, P. F. TORTORELLI AND A. R. MARDER

ABSTRACT. Single-pass welds and multiple-pass cladding of Fe-Al alloys were deposited on carbon steel substrates using the gas tungsten arc and gas metal arc welding processes. The effect of alloy composition on cold cracking susceptibility was assessed using a dye penetrant technique. The high-temperature (600°C) sulfidation behavior of low-Al alloys (5–10 wt-% Al), which exhibited good weldabilty, was examined using a thermogravimetric balance in a moderately reducing 0.1% H_2S–3.0% H_2–bal. Ar gas. Microstructural characterization was conducted by light optical microscopy, scanning electron microscopy, electron probe microanalysis and Knoop hardness testing. By varying the welding parameters, a range of dilution levels was achieved that resulted in fusion zone compositions with 3–30 wt-% Al. Under these processing conditions, cracking of the Fe-Al cladding is directly related to the aluminum concentration within the deposit. Cracking of the cladding was seen to have occurred by both inter- and transgranular modes for deposits containing greater than 10 wt-% Al. Below this composition limit, cracking did not occur. According to the Fe-Al phase diagram, this composition indicates the microstructural transition from the single-phase region of disordered solid solution (α) to the two-phase region of α + ordered Fe_3Al. The ordered structures of Fe_3Al and FeAl have been found to be more susceptible to environmental embrittlement, which has been seen to be the source of the cladding cracking problem. In terms of sulfidation behavior, alloys containing 5–10 wt-% Al exhibited corrosion rates significantly lower than carbon steel and 304 stainless steel. The results of this work indicate that Fe-Al cladding containing 5–10 wt-% Al shows potential promise for applications requiring a combination of weldability and sulfidation resistance in moderately reducing environments.

S. W. BANOVIC, J. N. DuPONT and A. R. MARDER are with the Department of Materials Science and Engineering, Lehigh University, Bethlehem, Pa. P. F. TORTORELLI is with Oak Ridge National Laboratory, Oak Ridge, Tenn.

Introduction

Intermetallic iron aluminide alloys based on the ordered structures of Fe_3Al and FeAl show excellent resistance to oxidation and sulfidation in highly aggressive environments (Refs. 1–8). This outstanding resistance has been attributed to the formation of a dense, adherent surface scale of aluminum oxide (Al_2O_3) that is stable under a wide range of environments. In order to utilize their excellent corrosion resistance and avoid problems due to poor high-temperature strength (Ref. 1), the use of iron aluminide cladding has been considered. Recent work (Ref. 2) suggests that Al levels should be greater than approximately 9.6 wt-% for severely reducing environments (*e.g.*, 800°C, $P_{S2} = 10^{-6}$ atm, $P_{O2} = 10^{-22}$ atm). In spite of the potential protection offered, these compositions have been seen to be susceptible to hydrogen (cold) cracking (Refs. 9–11) subsequent to deposition. A direct correlation between the severity of embrittlement and the amount of aluminum in the alloy (Refs. 12–14) has been observed, specifically when the composition resides in the ordered regions of the Fe-Al phase diagram. Recent investigations (Refs. 10, 15) have cited the use of preheat and postweld heat treatments (PWHT) to alleviate some of the hydrogen cracking problem, thus allowing for higher aluminum content cladding to be deposited crack free. Regardless of these improvements, the use of such extensive treatments is usually not possible when coating large-scale structures. However, applications exist in which the corrosion environments are not as severely reducing and lower Al contents, which exhibit good weldability, may provide useful protection. A typical example includes the waterwall structures of coal-fired boilers operating with low NO_x burners (Refs. 16–18). These units often require cladding areas reaching up to 4000 ft^2 where application of preheat and PWHT are not possible. These units operate under a moderately reducing environment where low Al cladding may provide adequate protection. Successful substitution of currently used stainless steel and Ni alloy cladding by Fe-Al cladding would be accompanied by reduced cost and elimination of the brittle martensitic region that develops in the partially mixed zones of the cladding presently in use (Ref. 19). Thus, the objectives of this research are to investigate the weldability and sulfidation resistance of Fe-Al cladding in order to identify cladding compositions that offer a combination of good weldability and corrosion protection in mildly reducing environments.

KEY WORDS

Fe-Al Alloys
GTAW
GMAW
Cladding
Intergranular Cracking
Transgranular Cracking

Experimental Procedure

The cladding was produced using the gas tungsten arc (GTA) and gas metal arc (GMA) welding processes. For the GTAW process, a filler metal of commercially pure aluminum wire was directly fed into the weld pool. The substrates were A285 Grade C steel, 6 mm thick x 152 mm wide x 305 mm long. The filler metal feed speed and current were varied to pro-

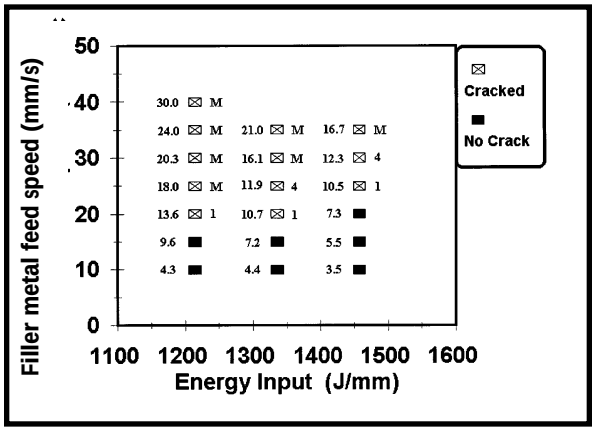

Fig. 1 — Sample matrix of single-pass welds produced by GTAW. Each box represents a sample deposited at that processing condition and was subsequently labeled as cracked or no crack. Numbers to the right of the cracked data points signify the number of cracks that occurred, with M being more than 15. The numbers to the left denote the wt-% of aluminum in the deposit.

duce different aluminum concentrations in the cladding. A constant travel speed of 2.0 mm/s was used for all GTAW experiments. Single- and multiple-pass deposits were produced under identical processing parameters using argon shielding gas. For the GMAW multiple-pass welds, a range of values for electrode tip-to-plate distance, electrode feed speed and travel speed was used. The electrode tip-to-plate distance was varied in order to induce current variations within a fixed electrode feed speed. Two aluminum-cored, steel-sheathed wires with different amounts of aluminum (13 and 27 wt-%) were used as the consumable electrodes, and a shielding gas of Ar-2% O_2 was utilized. To simulate the external constraint encountered during welding, the steel plates were restrained by bolts placed in each of the four corners. Preheat and postweld heat treatments were not conducted, but an interpass temperature for the multiple-pass welds was maintained between 300° and 350°C. A dye penetrant technique was used to assess cracking of the cladding.

Samples were removed from the cladding using an abrasive cutoff wheel, mounted in cold-setting epoxy and polished to a 0.04-μm finish using colloidal silica. The samples were etched in a solution of 60 mL methanol, 40 mL nitric acid and 20 mL hydrochloric acid. Microstructural characterization was performed using light optical microscopy (LOM) and scanning electron microscopy (SEM). Electron probe microanalysis (EPMA) was conducted on a JEOL 733 SuperProbe equipped with wavelength dispersive spectrometers. The accelerating voltage and probe current were 15 kV and 15 nA, respectively. K_α X-ray lines were analyzed and counts converted to weight percentages using a ϕ (ρz) correction scheme. Knoop hardness measurements were made with a LECO hardness tester using a load of 100 g held for 15 s.

To simulate various cladding compositions and simultaneously provide bulk samples for corrosion testing, cast iron-aluminum alloys were produced by arc melting high-purity components under argon and drop casting into a water-cooled copper mold. Based on the weldability results, alloy compositions of 5, 7.5 and 10 wt-% Al were prepared. The use of cast samples to study the sulfidation behavior of cladding is based on previous work that has shown that the corrosion behavior of Fe-Al cladding could be explained on the basis of what was known from cast alloys of equivalent composition (Refs. 6, 7).

High-temperature sulfidation corrosion behavior was characterized by use of a Netsch STA 409 high-temperature thermogravimetric balance that measured weight gain as a function of time. Corrosion samples were ground to 600 grit with silicon carbide papers and ultrasonically cleaned before being placed in the balance. The samples were heated at a rate of 50°C/min and isothermally held at 600°C for 50 h in a mixed gas consisting of 0.1% H_2S-3.0% H_2-bal. Ar (by volume). This H_2S content is similar to that recently measured in coal-fired power plants operating with Low NO_x burners (Refs. 16–18). The oxygen partial

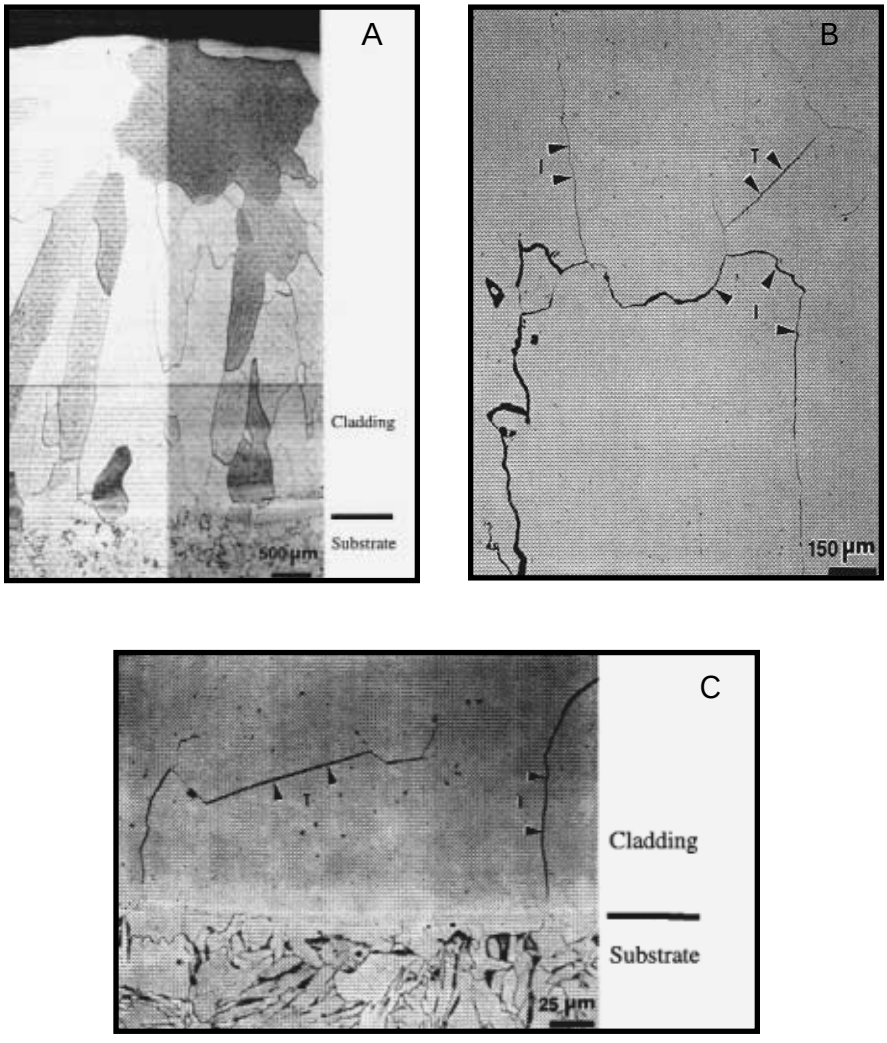

Fig. 2 — A — Typical columnar microstructure of GTAW cladding; B — cracking is seen to occur by both inter- (I) and transgranular (T) modes; and C — cracking is arrested at the weld interface.

pressure, as determined by a solid-state oxygen cell, was 10^{-28} atm, and the sulfur partial pressure was calculated to be 10^{-9} atm. After exposure, samples were cooled to room temperature at a rate of 20°C/min. Microstructural characterization of the corrosion samples was performed using scanning-electron microscopy (SEM) and energy dispersive spectrometry (EDS).

Results and Discussion

GTAW Single-Pass Deposits

A sample matrix was produced to obtain a wide range of aluminum contents and determine the maximum amount of aluminum that could be tolerated in the cladding without cracking. Filler metal feed speeds between 10 and 50 mm/s were used while the current was varied between 250 and 300 A in 25-A increments. Voltages averaged around 14.5 V. Single-pass welds were first deposited to ensure that the microstructure and compositions of the cladding were not complicated by overlapping passes. Figure 1 shows the experimental matrix of the single-pass deposits. The energy input was calculated using an arc efficiency of 0.67 for the GTAW process (Ref. 20). Each data point represents a cladding deposited and is labeled as either cracked or not cracked. For those that cracked, the number of cracks that occurred are located to the right of the symbols, with M signifying more than 15. The numbers to the left of the symbols denote the amount of aluminum in the deposit (in wt-%) as measured using EPMA. The samples located near the crack/no crack boundary exhibited reproducible cracking tendencies. Cracking of the welds was observed to occur soon after solidification as well as days after depositing the cladding.

All of the deposits produced with this range of processing conditions exhibit coarse columnar microstructures — Fig. 2A. Cracking of the cladding was both inter- and transgranular — Fig. 2B. As shown in Fig. 2C, cracks in the deposits never propagated into the underlying substrate, but appear to be arrested at or near the interface. Composition traces across the columnar microstructures of three deposits prepared at a constant energy input and varying filler metal feed speeds are shown in Fig. 3. The size of the partially mixed zone (PMZ) is seen to increase as the nominal aluminum content of the weld increases. A typical composition profile acquired across a single grain is shown in Fig. 4. These results show that, beyond the PMZ, the deposits exhibit a uniform distribution of alloying elements. These results indicate that good mixing occurs beyond the PMZ and that localized concentration gradients, which typically develop due to microsegregation, are eliminated during solidification and post-solidification cooling. The elimination of localized concentration gradients, as seen in Fig. 4, can be attributed to the relatively high diffusivity of Al in the BCC structure of disordered solid solution (α).

The size of the PMZ generally increases with increasing filler metal feed rate. This indicates that the thickness of the stagnant boundary layer near the weld interface increases as the filler metal feed rate increases. However, beyond this point, the composition is uniform. For cladding with Al contents below 10 wt-% that exhibit good weldability, the partially mixed zone is small compared to the deposit thickness. These results are significant because they indicate there should be no regions near the surface of the deposits that are Al depleted; thus, there should be no regions susceptible to localized corrosion.

Figure 5 shows a typical Knoop hardness trace across the weld interface of an Fe-Al alloy. No significant spike in hardness occurs near the weld interface indicative of a brittle interface layer, as commonly seen with stainless steel and nickel-alloy cladding (Ref. 19). During deposition of the super alloys, a composition gradient between the base metal and weld metal may form, lead-

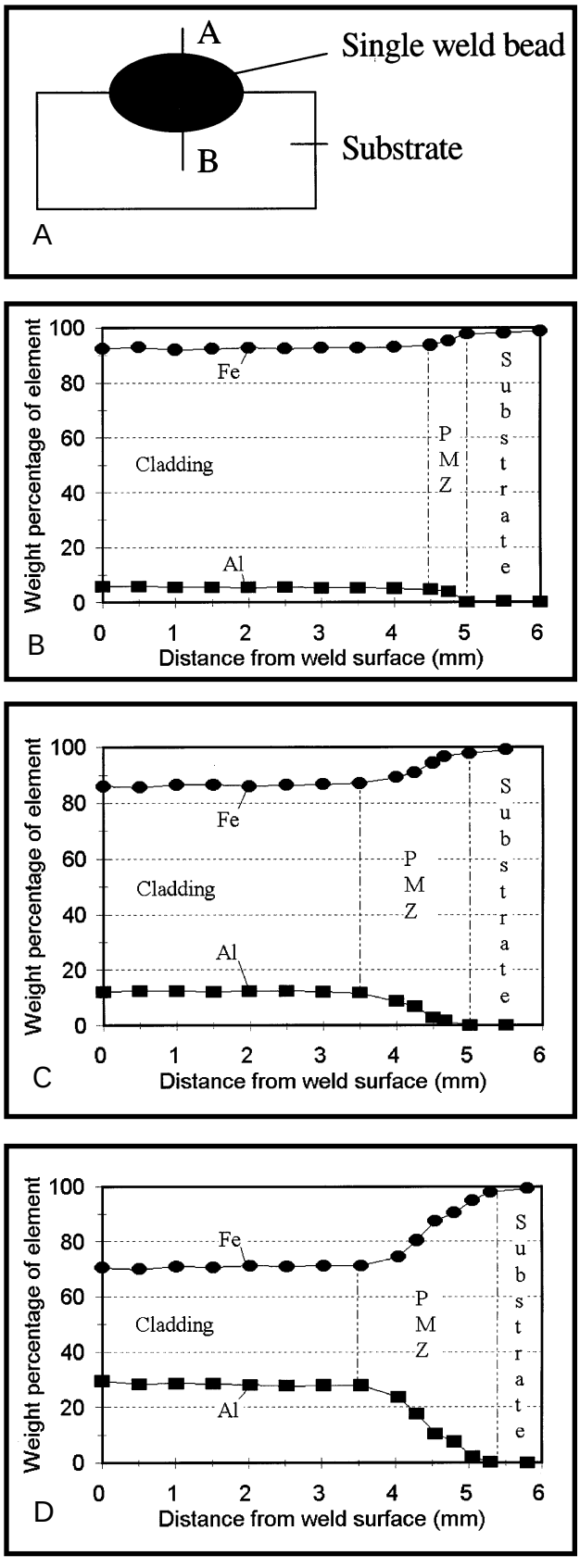

Fig. 3 — Composition EPMA traces through single-pass GTAW deposits. A — Traces were conducted perpendicular to the deposit/substrate interface. The size of the partially mixed zone (PMZ) is seen to increase as the nominal aluminum content of the weld increases; B — 5.5 wt-% Al; C — 12.3 wt-% Al; D — 28.4 wt-% Al.

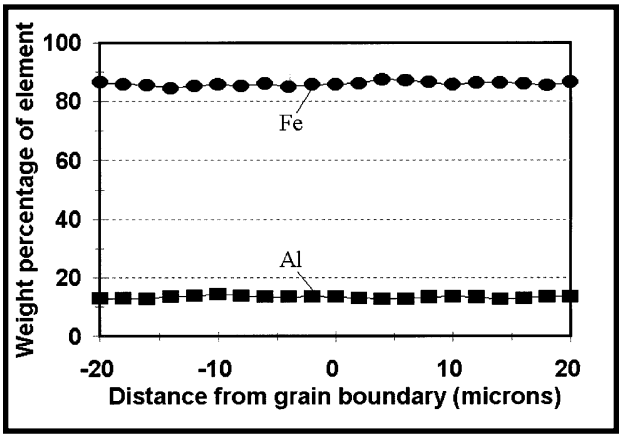

Fig. 4 — Composition EPMA trace across a grain boundary showing no localized concentration gradient.

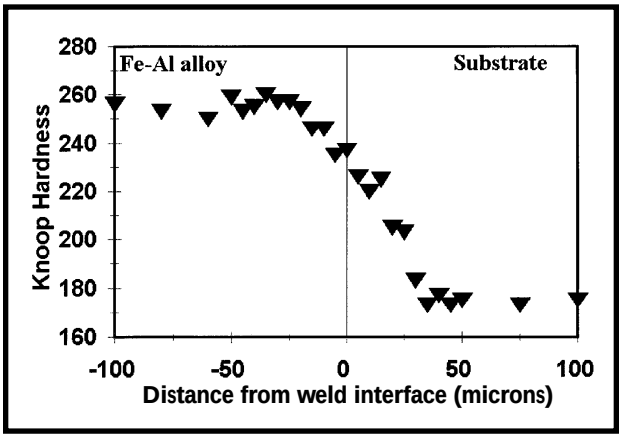

Fig. 5 — Typical Knoop hardness profile across the weld interface of a cladding with nominal aluminum content of 7.2 wt-%.

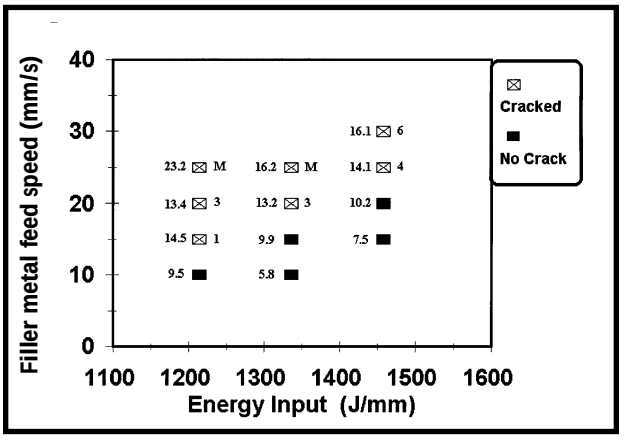

Fig. 6 —Sample matrix of GTAW multiple-pass cladding. The symbols correspond to those in Fig. 1.

ing to complex microstructures close to the weld interface. With relatively high cooling rates, the formation of a martensitic layer, which is high in strength and low in ductility, is often observed in this area. Gittos and Gooch (Ref. 19) observed that this hard zone cracked during side bend tests, thus lending the possibility of the brittle interface layer being susceptible to cracking under thermal cycling conditions.

Figure 1 shows that the amount of aluminum in the deposit decreases with increasing energy input and decreasing wire feed speed. This trend is readily expected and can be interpreted based on the simple energy balance dilution model recently proposed by DuPont and Marder (Ref. 20). The dilution is essentially controlled by the relative melting rates of the filler metal and substrate. For a fixed filler metal feed rate (melting rate), the dilution increases (*i.e.*, amount of Al decreases) with increasing energy input. In this case, the extra energy cannot be absorbed by the filler metal if the filler metal feed rate is fixed, so the substrate absorbs the extra energy. This results in an increase in the melting rate of the substrate and a concomitant increase in dilution. Conversely, for a given energy input, an increase in the filler metal feed rate results in a decrease in dilution (*i.e.*, higher Al). Here, the filler metal consumes a larger portion of the total energy input and less energy is available to melt the substrate. As a result, the substrate melting rate decreases and dilution is reduced. Figure 1 shows that a dilution level resulting in approximately 10 wt-% Al in the cladding represents a boundary condition. Processing conditions below this boundary produced cladding with less than 10 wt-% Al that did not crack under the current set of conditions, while cladding produced with parameters above the boundary exhibited greater than 10 wt-% Al and were susceptible to cracking.

Previous studies (Refs. 9, 10) have shown that iron aluminide cladding with ordered structures (*i.e.*, Fe_3Al and FeAl) are susceptible to hydrogen-induced (cold) cracking due to environmental embrittlement enhanced by residual stresses from welding. Intrinsically, bulk iron aluminides have been observed to be quite ductile when tested in vacuum or dry oxygen atmosphere at room temperature (Refs. 21–24). However, the ductility dramatically decreases when tested in atmospheres containing moisture. This is attributed to environmental embrittlement involving hydrogen generated from the chemical reaction between aluminum and water vapor (Ref. 25):

$$2Al + 3H_2O \rightarrow Al_2O_3 + 6H^+ + 6e^- \quad (1)$$

The atomic hydrogen is produced at the crack tip and then enters the lattice, propagating ahead of the advancing crack and reducing the ductility of the alloy. This evolution and transport of hydrogen, when combined with the residual stresses that exist during and after welding (Ref. 26), promote hydrogen cracking. Previous studies (Ref. 15) have shown that preheat and postweld heat treatments can be utilized to produce crack-free intermetallic alloys with aluminum concentrations around 15.9 wt-%. However, under conditions where preheat and PWHT are not possible, the results in Fig. 1 indicate that the Al content in the cladding should be below 10 wt-%.

Other researchers (Refs. 12–14) have observed a similar trend for bulk samples. For example, Sikka, *et al.* (Ref. 13), have shown that a wrought Fe-Al alloy with 8.4 wt-% Al, which has a disordered structure, exhibits a ductility (elongation) above 20% when tested in air. However, when the Al content is increased to 12 wt-% and above, the ductility drops significantly to approximately 5%. This trend is in good agreement with the weldability results presented in Fig. 1. According to the Fe-Al phase diagram, those claddings that did not crack are located in the single-phase, disordered α region. The ordered-phase Fe_3Al is first observed approaching 10 wt-% Al, leading to a dual-phase, ordered Fe_3Al + disordered solid solution α deposit and, as seen in Fig. 1, the onset of cladding cracking. It must be emphasized that these results

should be considered tentative as the sensitivity to hydrogen cracking will also depend on, for example, the degree of restraint as affected by the substrate size. The small-scale results presented here are intended to serve as a guide for further research and subsequent practical applications. The reproducibility of these results to multiple-pass deposits produced with both the GTAW and GMAW processes is discussed below.

GTAW Multiple-Pass Cladding

Based upon the single-pass results, a second experimental matrix of multiple-pass cladding was produced using similar parameters — Fig. 6. As found for the single-pass welds, the cracking results were again related to the amount of aluminum in the cladding. Due to the 50% overlap of adjacent passes, the aluminum contents of the multiple-pass cladding were higher than that of the corresponding single-pass welds prepared at identical processing parameters. Microstructures for these samples were similar to those found for the single-pass deposits, as seen in Fig. 2, and cracking was again observed to occur in both inter- and transgranular modes. Electron microprobe traces through the multiple-pass cladding, conducted parallel to the coating-substrate interface, showed the cladding was homogeneous on a macroscopic scale at these processing parameters — Fig. 7. Again, cladding compositions on either side of the crack/no crack boundary for the matrix exhibited reproducible cracking tendencies.

GMAW Multiple-Pass Cladding

Multiple-pass cladding was deposited with the GMAW process using a range of currents between 260 and 370 A. Current variations were achieved by changes to both the electrode feed speed and electrode tip-to-plate distance. In addition, two aluminum-cored, steel-sheathed wires with different amounts of aluminum (13 and 27 wt-%) were used as consumable electrodes to alter the compositions of the deposits. Figure 8 shows the experimental matrix for the cladding produced. A value of 0.87 was used for the arc efficiency to calculate the energy input (Ref. 20). All deposits produced with the 27 wt-% Al electrode resulted in cladding with more than 15 cracks (above dashed line in Fig. 8). Use of this electrode resulted in deposits with higher aluminum contents, even when relatively high energy inputs were used. The dilution levels for both electrodes ranged between 40 and 50%, which is much lower than the range attained for GTAW. Unlike the GTAW process, the GMAW current and electrode feed speed cannot be changed independently under the current set of conditions. As a result, it is difficult to achieve a higher range of dilution levels. This made it difficult to produce cladding with composition near 10 wt-% Al. However, for the cladding produced under these conditions, the weldability results are in agreement with those of Figs. 1 and 6, where cladding with less than 10 wt-% Al could be deposited crack free. Like the GTAW deposits, the cladding microstruc-

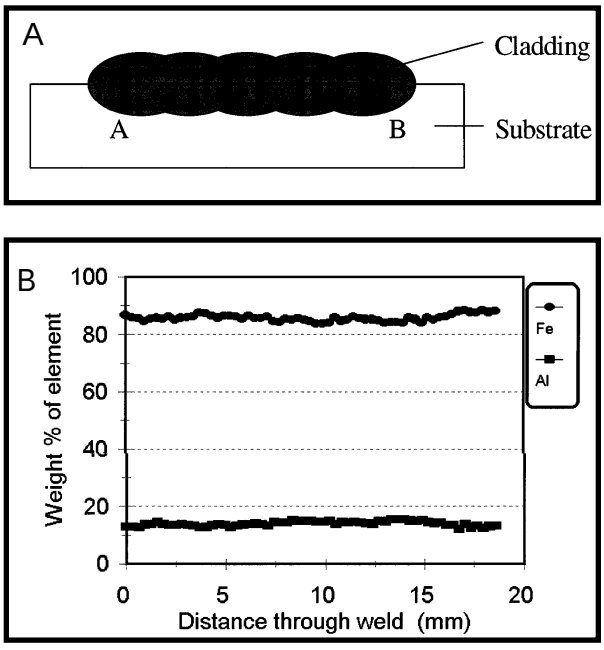

Fig. 7 — Typical composition EPMA trace through a multiple-pass cladding showing the deposit is homogeneous on a macroscopic scale. Trace was conducted parallel to the coating/substrate interface as seen in A.

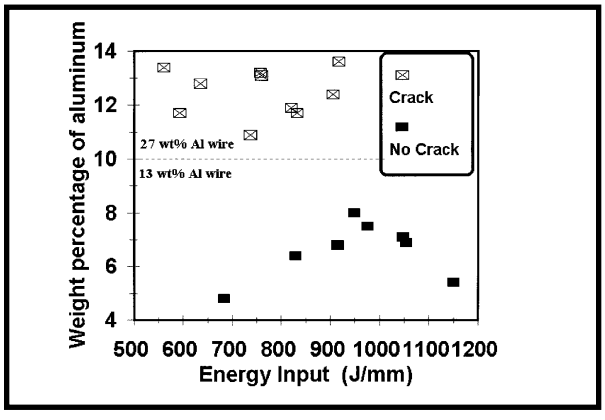

Fig. 8 — Sample matrix of multiple-pass cladding produced by GMAW. The dashed line signifies the difference between the two types of aluminum-cored, steel-sheathed wires. Above the line, the 27 wt-% Al wire was used to produce the cladding, while below the 13 wt-% Al wire was deposited. All samples that cracked had in excess of 15 cracks per deposit.

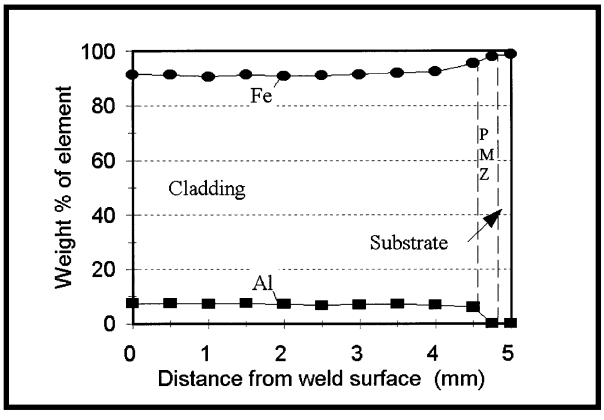

Fig. 9 — Typical probe trace through a multiple-pass GMAW cladding. Trace was taken perpendicular to the coating/substrate interface.

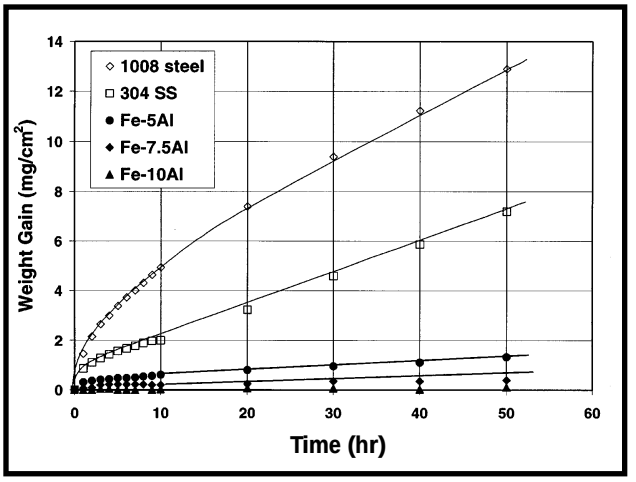

Fig. 10 — Weight change vs. time for commercial and cast Fe-Al alloys exposed to 0.1% H_2S-3.0% H_2-bal. Ar at 600°C for 50 h (P_{S2} = 10^{-9}, P_{O2} = 10^{-28}).

tures had coarse columnar grains and a uniform composition beyond the partially mixed zone — Fig. 9.

Sulfidation Behavior

Fe-Al alloys were cast to produce nominal aluminum contents of 5, 7.5 and 10 wt-% Al. This composition range was chosen based on the weldability studies. From the work of Tortorelli, *et al.* (Refs. 6, 7), it was shown that the oxidation/sulfidation resistance of iron aluminide cladding could be explained on the basis of what was known from previous studies of bulk samples of similar compositions. The corrosion environment chosen in this current work was generally less aggressive than those presently found in the literature (Refs. 6–8, 27–32) in terms of gas composition and temperature, so as to be more representative of applications with moderately reducing environments (Refs. 16–18). Previous work (Ref. 2) on binary Fe-Al alloys showed that up to ~750°C, at least 9.6 wt-% is needed for good sulfidation resistance in severely reducing environments.

The weight changes for the alloys tested are shown in Fig. 10. The 5 wt-% alloy was the only one that displayed a significant weight gain among the Fe-Al alloys, which nearly tripled that of the other two tested. The linear kinetic rate constant for this alloy (k_l = 3.2 x 10^{-4} mg cm^{-2} min^{-1}) was less than those previously reported (Ref. 30) for similar alloys in more aggressive conditions (k_l = 7.1 x 10^{-2} mg cm^{-2} min^{-1}). The 7.5 and 10 wt-% alloys had negligible weight gain, especially when compared to Type 304 stainless steel and Type 1008 carbon steel. The weight gain measurements can be correlated with SEM micrographs of the sample surfaces — Fig. 11. The amount of surface corrosion product decreases as the aluminum content increases in the alloy. The 5 wt-% sample has a scale that completely covered the surface and EDS techniques detected iron and sulfur — Fig. 12A. The scale morphology, consistent with previous research (Refs. 30, 31), in addition to the EDS spectra, suggests an iron sulfide scale is present. An aluminum peak was not present in the spectra, indicating that the iron sulfide scale is either a few microns thick, since the interaction volume is ~1 μm with these SEM parameters (Ref. 33), or very little aluminum is present in the reaction product. The 7.5 wt-% alloy had few large iron sulfide particles on the surface (Fig. 11B), with the presence of iron and sulfur peaks in the EDS spectra — Fig. 12B. The 10 wt-% alloy was devoid of any large particles (Fig. 11C) and Fig. 12C shows the spectra containing all three peaks (Fe, Al and S). Due to limitations of the EDS system, oxygen could not be detected to determine if the formation of any oxides occurred.

The 600°C Fe-S-O and Al-S-O thermodynamic stability diagrams are shown superimposed on each other in Fig. 13, and the partial pressures of sulfur and oxygen utilized for this research are noted in the figure. Based on these considerations, formation of iron sulfide and aluminum oxide is favored on the alloy surface. It should be noted here, however, that care should be taken when using these diagrams

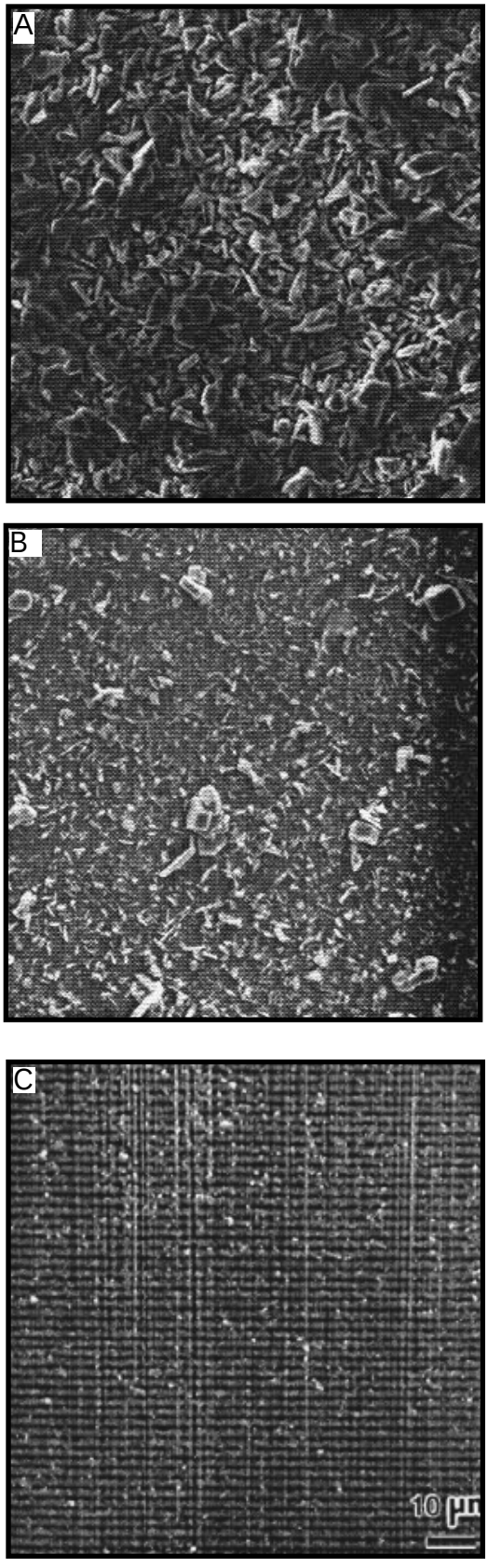

Fig. 11 — SEM micrograph showing the corroded surface of Fe-Al alloys containing the following: A — 5 wt-% Al; B — 7.5 wt-% Al; and C — 10 wt-% Al.

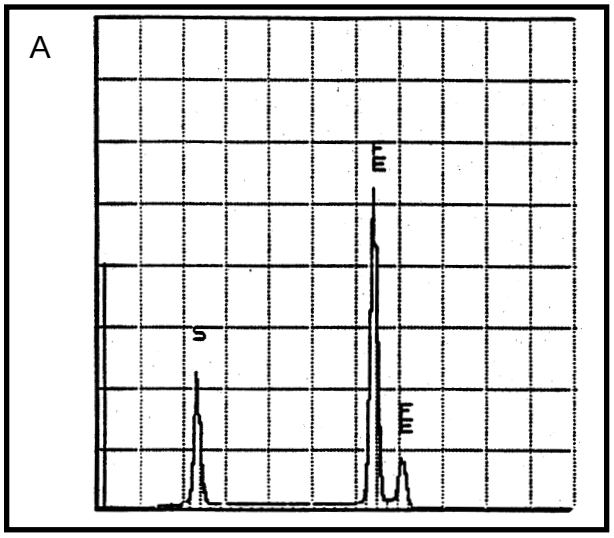

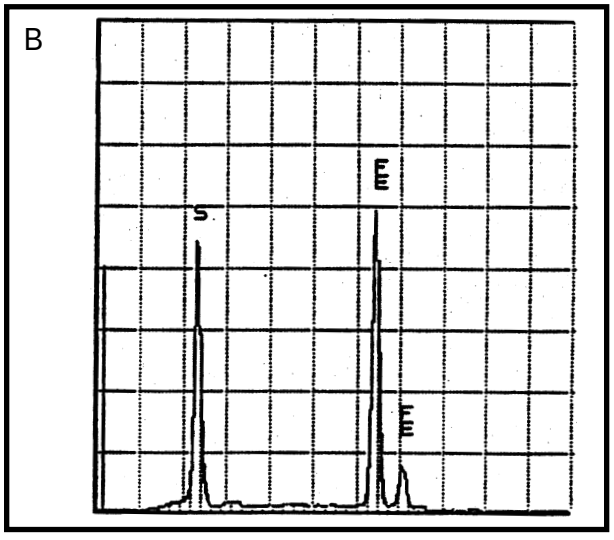

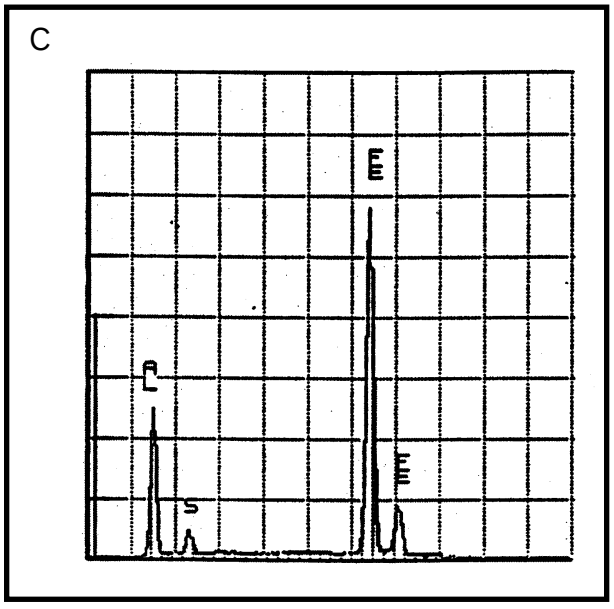

Fig. 12 — EDS spectra indicating elements detected in the surface scale of alloys containing the following: A — 5 wt-% Al; B — 7.5 wt-% Al; and C — 10 wt-% Al.

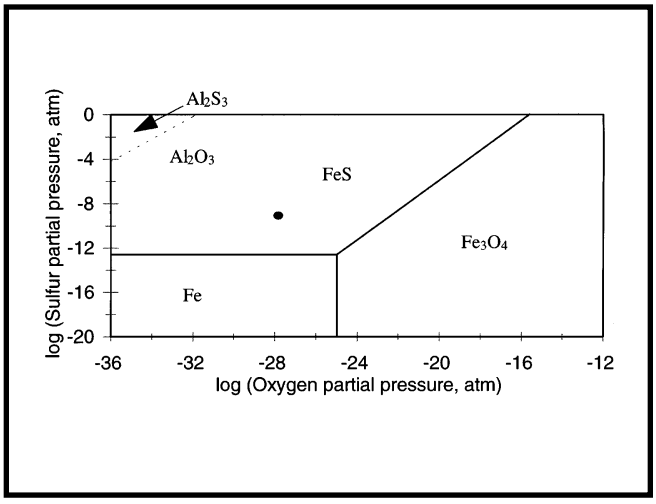

Fig. 13 — Thermodynamic stability diagrams for Fe-O-S (solid lines) and Al-O-S (dashed line) at 600°C superimposed on each other. The conditions used in this research are marked by the ●.

to predict which phases may form in the given environment. The construction of these diagrams considers only thermodynamic relationships at equilibrium and neglects the kinetic rates of the scales forming. Therefore, it is possible that a faster growing and less stable scale may prevent the formation of a continuous, protective one. This may explain the result found in this research. Although not experimentally observed, the low weight gains could be due in part to the formation of an alumina surface scale on the Fe-Al alloys. DeVan and coworkers (Refs. 1–8, 34) have previously shown that the formation of this scale provided iron aluminides with excellent corrosion resistance due to its thermodynamic stability and relatively slow growth. The scales were found to be thin and adherent in isothermal conditions. This same type of scale may be present, but undetected, on the Fe-Al alloys, thus giving them their good corrosion resistance. The low corrosion rates, combined with good weldability, makes the disordered Fe-Al alloys potential candidates for corrosion protection in applications with moderately reducing environments.

Conclusions

From this study of the weldability and high-temperature sulfidation resistance of Fe-Al alloys, the following conclusions can be drawn.

1) Using GTAW and GMAW processes, single- and multiple-pass claddings of Fe-Al were produced with aluminum contents ranging from 3 to 30 wt-%. All claddings were found to have a columnar microstructure that was relatively homogenous on a microscopic scale throughout the bulk of the fusion zone. A partially mixed zone was located near the weld interface that increased in size as the nominal aluminum content of the cladding increased.

2) Under these processing conditions, cracking of the Fe-Al cladding, both inter- and transgranular, was found to be independent of the welding process and parameters. Instead, cracking was directly related to the amount of aluminum in the deposit. Above 10 wt-% Al, cracking was seen to be prevalent throughout the cladding. This composition corresponds to the microstructural transition from the single-phase, disordered solid solution α to α + ordered Fe_3Al. It has previously been observed that the ordered structures (Fe_3Al, FeAl) are more susceptible to environmental embrittlement, which is the source of the cladding cracking problem.

3) Excellent sulfidation behavior in moderately reducing environments was

found for alloys containing 5 to 10 wt-% Al. These compositions also exhibited good weldability, which may make them potential candidates for cladding materials.

Acknowledgments

This research was sponsored by the Fossil Energy Advanced Research and Technology Development (AR&TD) Materials Program, U.S. Department of Energy, under contract DE-AC05-96OR22464 with Lockheed Martin Energy Research Corp. The authors wish to thank A. O. Benscoter for his aid in metallographic preparation and V.K. Sikka at Oak Ridge National Laboratories for the cast Fe-Al alloys used in corrosion testing.

References

1. McKamey, C. G., DeVan, J. H., Tortorelli, P. F., and Sikka, V. K. 1991. *Journal of Materials Research* 6(8): 1779–1805.

2. DeVan, J. H., and Tortorelli, P. F. 1993. *Materials at High Temperature*, 11(1–4), pp. 30–5.

3. Tortorelli, P. F., and DeVan, J. H. 1992. *Mat. Science and Engineering* 135A (1–2): 573–577.

4. DeVan, J. H., and Tortorelli, P. F. 1993. *Corrosion Science* 35(5–8): 1065–1071.

5. Tortorelli, P. F., and DeVan, J. H. 1994, *Processing, Properties, and Applications of Iron Aluminides*, pp. 257–270. TMS, Warrendale, Pa.

6. Tortorelli, P. F., Goodwin, G. M., Howell, M., and DeVan, J. H. 1995. *Heat-Resistant Materials II*, pp. 585–590. Gatlinburg, Tenn. ASM, Materials Park, Ohio.

7. Tortorelli, P. F., DeVan, J. H., Goodwin, G. M., and Howell, M. 1994. *Elevated Temperature Coatings: Science and Technology I*, pp. 203–212, Rosemont, Ill. TMS, Warrendale, Pa.

8. DeVan, J. H., and Tortorelli, P. F. 1992. High temperature corrosion of iron aluminides, *Corrosion 92*, Paper 127.

9. David, S. A., Horton, J. A., McKamey, C. G., Zacharia, T., and Reed, R. W. 1989. *Welding Journal* 68(9): 372-s to 381-s.

10. Maziasz, P. J., Goodwin, G. M., Liu, C. T., and David, S. A. 1992. *Scripta Metallurgica et Materialia* 27(12): 1835–1840.

11. Fasching, A. A., Ash, D. I., Edwards, G. R., and David, S. A. 1995. *Scripta Metallurgica et Materialia* 32(3): 389–394.

12. Woodyard, J. R., and Sikka, V. K. 1993. *Scripta Metallurgica*, 29, pp. 1489–1493.

13. Sikka, V. K., Viswanathan, S., Vyas, S. 1993. High temperature ordered intermetallic alloys V. *Materials Research Society Symposium Proceedings*, Vol. 28, pp. 971–976. Eds. I. Baker, R. Darolia, J. D. Whittenberger and M. H. Yoo. Materials Research Society, Pittsburgh, Pa.

14. Vyas, S., Viswanathan, S., and Sikka, V. K. 1992. *Scripta Metall.,* 27, p. 185.

15. David, S. A., and Zacharia, T. 1991. Heat-resistant materials, *Proceedings of the 1st International Conference*, pp. 169–173, Fontana, Wis.

16. Chou, S. F, Daniel, P. L., Blazewicz, A. J., and Dudek, R. F. 1984. Hydrogen Sulfide Corrosion in Low NOx Combustion Systems. Presented to the Metallurgical Society of AIME, Detroit, Mich. Babcock & Wilcox report # RDTPA 84-12.

17. Urich, J. A., and Kramer, E. 1996. *1996 International Joint Power Generation Conference*, Vol. 1, pp. 25–29, ASME, EC-Vol. 4/FACT-Vol. 21.

18. Gabrielson, J. E., and Kramer, E. D. 1996. *1996 International Joint Power Generation Conference*, Vol. 1, pp.19–23, ASME, EC-Vol. 4/FACT-Vol. 21.

19. Gittos, M. F., and Gooch, T. G. 1992. *Welding Journal* 71(12): 461-s to 472-s.

20. DuPont, J. N., and Marder, A. R. 1996. Welds, *Metallurgical and Materials Transactions B*, 27B, pp.481–499.

21. Liu, C. T., Lee, E. H., and McKamey, C. G. 1989. *Scripta Metallurgica*, 23, pp. 875–880.

22. Lui, C. T., McKamey, C. G., and Lee, E. H. 1990. *Scr. Metall.* 24: 385–390.

23. Lui, C. T., Fu, C. L., George, E. P., and Painter, G. S. 1991. ISIJ International 31, pp. 1192.

24. Stoloff, N. S., and Duquette, D. J. 1993. *Journal of Metals*, Dec., pp. 30–35.

25. Speidel, M. P. 1977. *Hydrogen Damage*, ed. C. D. Beachem. ASM Publication, pp. 329–351.

26. Wang, X. L., *et al. Mat. Res. Soc. Symp. Proc.* Vol. 364, Materials Research Society, pp. 109–114.

27. Strafford, K. N., and Manifold, R. 1972. *Oxidation of Metals* 5(2) 85–112.

28. Patnaik, P. C., and Smeltzer, W. W. 1985. *J. of the Electrochemical Society*, 132, pp. 1226–1232.

29. Smith, P. J., and Smeltzer, W. W. 1987. *Oxidation of Metals* 28: 291–297.

30. Strafford, K. N., and Manifold, R. 1969. *Oxidation of Metals* 1(2): 221–240.

31. DeVan, J. H., Hsu, H. S., and Howell, M. 1989. Sulfidation/Oxidation Properties of Iron-Based Alloys Containing Niobium and Aluminum, ORNL/TM-11176, Martin Marietta Energy Systems, Inc., Oak Ridge Natl. Lab.

32. Kai, W., and Huang, R. T. 1997. *Oxidation of Metals*, 48, pp. 59–86.

33. Goldstein, J. I., *et. al.* 1992. *Scanning Electron Microscopy and X-Ray Microanalysis*, 2nd Edition, pp. 87–90, Plenum Press, New York, N.Y.

34. DeVan, J. H. 1989. *Oxidation of High-Temperature Intermetallics*. Eds. T. Grobstein and J. Doychak, TMS, Warrendale, Pa. p. 107.

WRC BULLETIN 424

Bibliography of the Welding Reseach Supplements of the Welding Journal

Published in the American Welding Society
Welding Journal
From 1950–1996

Compiled by Robert La Pointe, Consultant

This document provides keyword listings of titles of technical papers that were published from 1950 to 1996 in the *Welding Journal's* Welding Research Supplement sponsored jointly by the American Welding Society and the Welding Research Council. The keyword list begins with numerical terms such as alloy designation and moves alphabetically to keywords as found in the titles. Each paper may appear in the listing several times.

Members of the Welding Research Council may obtain the same list in digital form by e-mail by contacting the Welding Research Council: wrc@forengineers.org.

Publication of this document — WRC Bulletin No. 424 — was sponsored by the Welding Research Council, Inc.

The price of **WRC Bulletin 424 (August 1997, 190 pages)** is $100.00 per copy plus $5.00 for U.S. and Canada and $10.00 for overseas postage and handling. Orders should be sent with payment to the Welding Research Council, 3 Park Avenue, 27th Floor, New York, NY 10016-5902. Phone (212) 591-7956; Fax (212) 591-7183; e-mail: wrc@forengineers.org; or visit our homepage http://www.forengineers.org/wrc.